ARKIV FÖR FYSIK Band 14 nr 32

Communicated 4 June 1958 by Bengt Edlén and Torsten Gustafson

Energy and angular distribution of scattered radiation in a water tank irradiated by X-rays

By G. Hettinger and N. Starfelt

With 11 figures in the text

SUMMARY

The spectral distribution of scattered X-rays in different directions in a water phantom was studied with the aid of a NaI(Tl) scintillation spectrometer. The primary radiation consisted of heavily filtered X-rays from a commercial X-ray generator with a maximum voltage of 300 kV. The experimentally determined spectra, differential in energy and angle, were integrated over all angles to give the photon number flux at different primary energies and water depths.

Introduction

The passage of X-rays through matter is accompanied by multiple Compton scattering. The photon flux at any point within an irradiated medium therefore consists not only of primary radiation but also of scattered photons. The present paper is concerned with an investigation with a point source outside a scattering medium, which is the most common geometrical configuration. The primary component of the photon flux is then monodirectional, whereas the scattered radiation comes from all parts of the irradiated material. The distribution in space and energy of the scattered X-rays is not only of interest for the study of buildup in broad beam geometry. In medical applications both the differential spectra and those integrated over all angles are required for a full understanding of the biological effect of the radiation at a given point.

Payne-Scott [1] calculated the theoretical energy distribution of first-order scattered radiation for primary photons with energies of radiological interest. Theoretical calculation of the spectra of multiply scattered radiation is difficult. The moment or polynomial method of Spencer and Fano [2, 3, 4] has proved useful. Depths to about 20 mean-free-path lengths can be studied. Using the SEAC electronic computer Goldstein and Wilkins [5] calculated energy spectra and buildup factors for the scattered radiation in different materials for different source energies and geometries. The scattering medium was assumed to be of infinite extent and the energy of the primary source ranged from 10 MeV down to about 250 kev. Recently Bruce and Johns [6] reported on Monte Carlo calculations of spectra of scattered radiation, that was produced in water by monoenergetic X-rays of interest in radiotherapy. Energy spectra at different dephts and for irradiated areas ranging from 25 cm^2 to infinity were calculated for primary energies of 50, 100, 200, 500, and 1250 kev. Other theoretical calculations of scattered gamma rays are given in the references [7–11].

An ionization chamber with known energy dependence can be used for the study of radiation quality. By this method the effective energy of scattered radiation in an irradiated phantom was studied by Quimby and others [12–15]. Greening [16] worked out a method for analyzing absorption data that gives an approximate spectrum of the scattered X-rays. He used spherical ionization chambers enclosed in shells of absorbing materials.

Some experimental investigations of the scattered radiation are on record in which a radioactive isotope, e.g. cobalt-60 was used as a primary source within a large water tank. White [17] and Van Dilla and Hine [18] studied the dose buildup and Hayward [19] measured the electron distribution with the aid of an anthracene crystal. Weiss and Bernstein [20] measured the spectrum of the scattered photons with a scintillation spectrometer. The energy region below 100 kev which corresponds to multiple scattering, was studied in detail. A similar technique was used by Theus *et al.* [21] in an investigation of the spectra of ceasium-137 gamma rays scattered in water. In an investigation by Peelle *et al.* [22] the energy and angular distribution of the total radiation was measured with a Compton crystal spectrometer.

In the above experiments the detector was placed inside the water tank. The displacement of water by the detector changes the photon flux from that found in a homogeneous medium. In a study of the spectrum of backscattered photons the spectrometer will shade the primary radiation to some extent.

Hayward and Hubbel [23] investigated the spectra of radiation backscattered by slabs of wood and steel wool irradiated by cobalt-60 gamma rays. They used a sodium iodide scintillation spectrometer and observed the low energy photons, which have undergone so many scattering processes as to have an isotropic distribution.

In the present investigation a NaI(Tl) scintillation spectrometer was used in the study of a beam of scattered radiation extracted in one of six different directions at three different depths on the central axis in a water phantom. The primary radiation consisted of heavily filtered X-rays from a commercial X-ray machine and was semi-monoenergetic (Hettinger and Starfelt [24]), with effective energies of 63, 113, and 184 kev. The experimentally determined spectra differential in energy and angle were integrated over all angles and, in order to secure absolute units, normalized with regard to the number of primary photons at the point of interest.

During the course of the present work a paper by Cormack *et al.* [25] appeared describing a similar investigation. As a radiation source they used a filtered beam with a half value layer of 3.8 mm Cu, from a 400 kVp X-ray generator. They made no attempt to measure the scattered radiation in absolute units.

There is, however, still a need for measurements of spectra of scattered radiation from semi-monoenergetic primary beams of several different energies. Such a set of data could provide a basis for the calculation of the spectra of the scattered radiation caused by any primary beam.

Experimental procedure

The experimental arrangement used in the study of X-rays scattered in water is shown in Fig. 1. The X-ray source was a MG 300 X-ray generator used at three different voltages, 100, 170, and 250 kV and supplied with filters to give semi-mono-

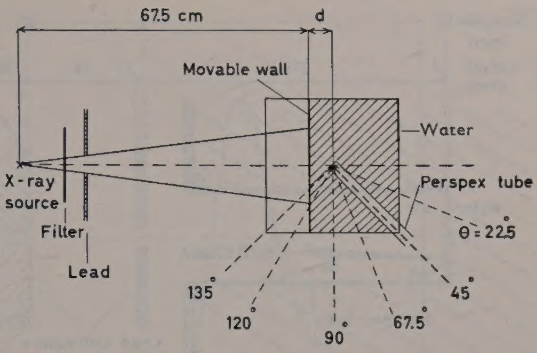

Fig. 1. Experimental arrangement for the study of scattered radiation in a water tank. The radiation was extracted through a narrow, empty perspex tube at six different angles.

energetic radiation. The spectra of the primary radiation are presented in Fig. 2. The X-ray source was kept at a constant distance of 67.5 cm from the entrance surface of the water phantom. Two different circular beam areas, 50 and 200 cm^2, respectively, at this surface were used in the experiment.

The water tank was a 30 × 30 × 30 cm^3 perspex tank with an adjustable front wall to permit measurement of the radiation spectrum at a fixed point on the central axis of the primary beam with various amounts of water, 2.5, 6.0, and 15 cm, interposed in the beam.

To study the radiation in the water without appreciably disturbing the spectrum, a beam of scattered X-rays was extracted from the point of interest through a narrow, empty perspex tube (Fig. 3). The end surface of this tube is on the cental axis of the primary radiation and defines the point to be studied. The collimation of the beam of X-rays was performed by means of two lead collimators placed outside the water

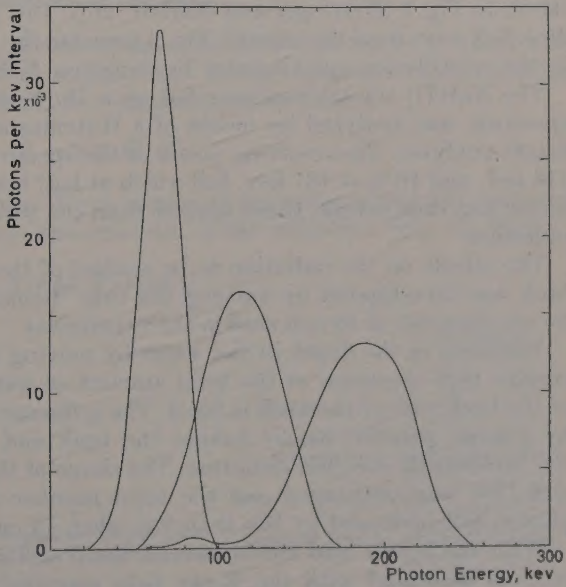

Fig. 2. Spectra of the primary radiation obtained by filtering the continuous radiation from a X-ray tube at accelerating potentials of 100, 170, and 250 kV. The areas of the curves are normalized to one photon.

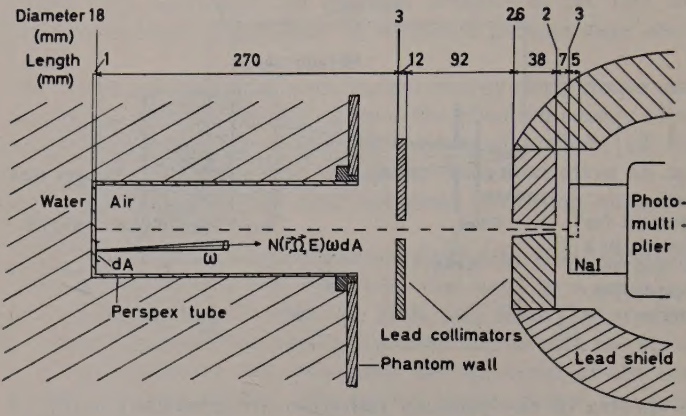

Fig. 3. The perspex tube and the scintillation spectrometer with the collimating system.

tank on a steel beam carrying the NaI(Tl) scintillation spectrometer, which was mounted inside a spherical lead shield, 4 cm thick. The perspex tube could be mounted at the angles 22.5, 45, 67.5, 90, 120, and 135 degrees to the primary beam and the spectrometer was rotated around a vertical axis through the point in which the radiation was studied.

108 spectra were measured with this arrangement. To decrease the amount of numerical computations it was thus desirable to simplify the corrections of the observed pulse height distributions as much as possible. Therefore the collimated beam of scattered X-rays was directed into the 37 mm diameter by 27 mm thick NaI(Tl) crystal through the bottom of a well, 3 mm in diameter and 5 mm deep as shown in Fig. 3 (Hettinger and Starfelt [26]). This prevented almost any escape of iodine *K* X-rays from the crystal. Fig. 4 presents the pulse height distribution produced in the scintillation spectrometer by tungsten *K* X-rays.

The NaI(Tl) crystal was mounted on a Du Mont 6292 photomultiplier. The pulse spectrum was analyzed by means of a Hutchinson–Scarrott type 100-channel pulse height analyzer. The resolving power of the spectrometer was 16 % at 65 kev, 12 % at 116 kev, and 10 % at 187 kev, full width at half height. The line width of the spectrometer was thus several times smaller than the width of the spectrum of the primary radiation.

The effects on the radiation to be studied of the empty perspex tube in the water tank was investigated by varying the tube diameter. It was found to be negligible for the diameter of 18 mm used in the experiment.

Variation in the depth in the water by moving the front wall of the perspex tank results in a variation of the total amount of water in the beam since the position of the back wall of the tank is fixed. The influence on the measurements was studied by placing paraffin blocks behind the tank and then remeasuring a spectrum of the backwardly directed radiation. The shape of the spectrum at 2.5 cm water depth and 135° was unchanged and the total number of scattered photons per primary photon was increased by less than 2 % when 15 cm of paraffin was inserted.

With the heavy lead shield around the NaI(Tl) crystal the background counting rate, as measured with the X-ray tube running, and with a lead absorber in the

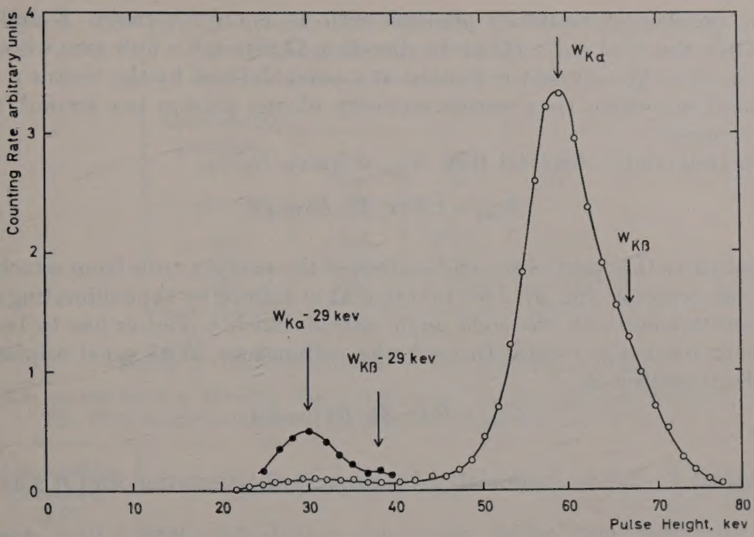

Fig. 4. The pulse height distribution produced in the scintillation spectrometer by tungsten *K* X-rays. The curve with the hollow circles represents the response when the beam is entering the crystal through the bottom of a well 3 mm in diameter and 5 mm deep. The solid circles show the *K* X-ray escape peak when using a crystal without a well.

scattered beam, was usually only a few per cent except at the greatest depth and smallest field size, but it was always below 40% of the counting rate when the absorber was removed.

Analysis of the data

The experimental pulse height distributions must be subjected to a number of calculations to yield the differential angular and energy spectrum of the photon number flux or, in abbreviated form, the angular number flux N

$$N = N(\mathbf{r}, \mathbf{\Omega}, E),$$

where $\mathbf{r}$ is the radius vector from the X-ray source to the point where the scattered radiation is observed and $\mathbf{\Omega}$ defines the direction of the radiation (Fig. 5). Thus

$$N(\mathbf{r}, \mathbf{\Omega}, E)\, d\Omega\, dE$$

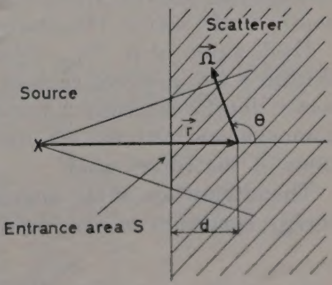

Fig. 5. Diagram illustrating the notations used for the spectra of scattered X-rays. In the experimental case the vector $\mathbf{r}$ is perpendicular to the entrance surface S.

means the number of scattered photons with an energy between E and $E+dE$ passing within the solid angle $d\Omega$ in the direction $\mathbf{\Omega}$ through a unit area whose normal is in the direction $\mathbf{\Omega}$ and that is located at a point defined by the vector $\mathbf{r}$. The flux is normalized according to a source intensity of one photon per second, assuming isotropic emission.

The experimentally observed flux N_{obs} is given by

$$N_{\text{obs}} = \int_A N(\mathbf{r}, \mathbf{\Omega}, E)\, \omega\, dA, \tag{1}$$

where A indicates that part of the end surface of the perspex tube from which photons can reach the detector (Fig. 3). The direction $\mathbf{\Omega}$ is defined by the collimating system of the spectrometer and ω is the solid angle within which a photon has to be directed to be able to reach the crystal through the collimators. With good approximation N_{obs} can be rewritten as

$$N_{\text{obs}} = N(\mathbf{r}, \mathbf{\Omega}, E) \int_A \omega\, dA. \tag{2}$$

The integral $\int_A \omega\, dA$ was calculated by numerical integration and it was found to be 1.34×10^{-5} ster. cm², which gave $(\omega)_{\text{av}} = A^{-1} \int \omega\, dA = 0.89 \times 10^{-5}$ steradian as the average value of ω.

The experimental spectra were corrected for the background counting rate. The limited resolving power of the spectrometer was disregarded since the recorded spectra are much broader than the line width. The well in the NaI crystal practically eliminates the K X-ray escape effect. Corrections were made for the crystal efficiency for energies above 150 kev and the spectrum of the primary radiation of highest energy was also corrected for the fact that the photofraction is less than 100 % at the upper end of this spectrum.

Finally the angular number flux was multiplied by $4\pi r^2 e^{\mu d}$ where r is the distance from the X-ray source, d that part of this distance that lies inside the water tank and μ the total absorption coefficient of the primary radiation. This is to be interpreted as a normalization of the number of scattered photons to one primary photon per cm² at the point studied. For each primary beam an effective or average value of $e^{\mu d}$ was calculated from the equation

$$(e^{-\mu d})_{\text{av}} = \frac{\int P(E) \cdot {}^{\exp(-\mu_E d)} \cdot dE}{\int P(E)\, dE}, \tag{3}$$

where $P(E)$ is the spectral distribution of the primary photons incident on the phantom surface (Fig. 2). Table 1 gives some data of the average values of $e^{-\mu d}$ at different depths in the water. The absorption coefficient, μ, was taken from White's tables [27].

Each value of $(e^{-\mu d})_{\text{av}}$ defines a monochromatic energy E_{eff} with the same $e^{-\mu d}$. Within a few per cent each of the primary beams has a constant effective energy for water depths between 2.5 and 15 cm. Consequently the primary beams are rather homogeneous with the effective energies listed in Table 2 together with the compositions of the filters used.

The integration of the angular number flux, N, over all angles gives the differential energy spectrum of the number flux or in abbreviated form, the number flux N_0

$$N_0 = N_0(\mathbf{r}, E) = \int^{4\pi} N(\mathbf{r}, \mathbf{\Omega}, E)\, d\Omega. \tag{4}$$

Table 1. The photon number transmission of the primary beams to different depths in water.

Accelerating potential (kV)	$e^{-\mu d}$		
	2.5 cm	6.0 cm	15 cm
100	0.608	0.300	0.0513
170	.662	.371	.0843
250	.704	.428	.1204

Table 2. Characteristics of the primary beams.

The radiation comes from a MG-300 X-ray generator with an inherent filtration of 4 mm Al. The filter combinations are the same as those used in reference [24].

Accelerating potential (kV)	Filter combination (mm)	E_{eff} (kev)	HVL (mm Cu)
100	1.67 Al, and 0.87 Cu	63	0.57
170	1.67 Al, 0.50 Cu, and 1.08 Cd	113	2.12
250	1.32 Al, 2.07 Cu, 1.10 Cd, and 1.34 Pb	184	4.50

Thanks to the rotational symmetry around the primary beam axis in the experimental case, the integral over the angles can be simplifed to

$$\int^{4\pi} N\,d\Omega = \int_0^{\pi}\int_0^{2\pi} N\ \sin\theta\,d\theta\,d\varphi = 2\pi\int_0^{\pi} N\ \sin\theta\,d\theta. \tag{5}$$

This integral was calculated with the aid of Lagrange's interpolation formula and Simpson's integral formula. If $N(\theta)$ is the photon distribution measured at the angle θ, N_0 can be written as

$$N_0 = \sum c_\theta \cdot N(\theta), \tag{6}$$

where c_θ includes $2\pi\sin\theta$ and the factor calculated from Simpson's formula. The different values of c_θ for the experimentally studied angles are given in Table 3.

It is possible to avoid the numerical work involved in the summation of eq. 6 by using the memory of a multichannel pulse height analyzer for direct addition of the differential spectra, which can be given the weights c_θ by using different exposure times.

Table 3. Constants for the weighted addition in eq. (6) in order to obtain the differential energy spectrum of the photon number flux.

θ	C_θ	θ	C_θ
22.5	1.26	90	2.13
45	1.16	120	2.26
67.5	3.04	135	2.38

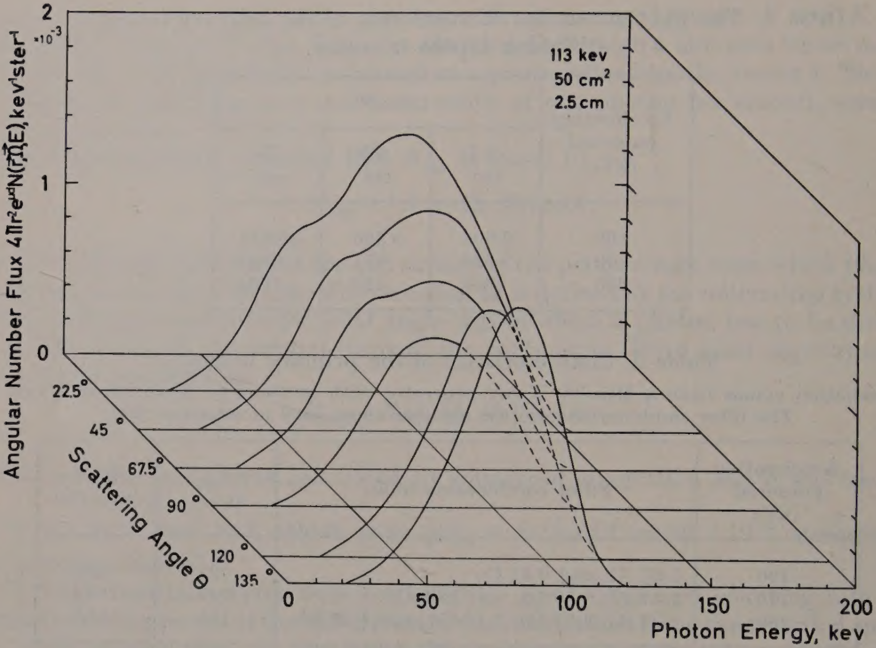
113 kev
50 cm^2
2.5 cm
Angular Number Flux $4\pi r^2 e^{\mu d} N(\vec{r}, \vec{\Omega}, E)$, kev^{-1}ster^{-1}
2
$\times 10^{-3}$
1
0
Scattering Angle Θ
22.5°
45°
67.5°
90°
120°
135°
0
50
100
150
200
Photon Energy, kev

6 a.

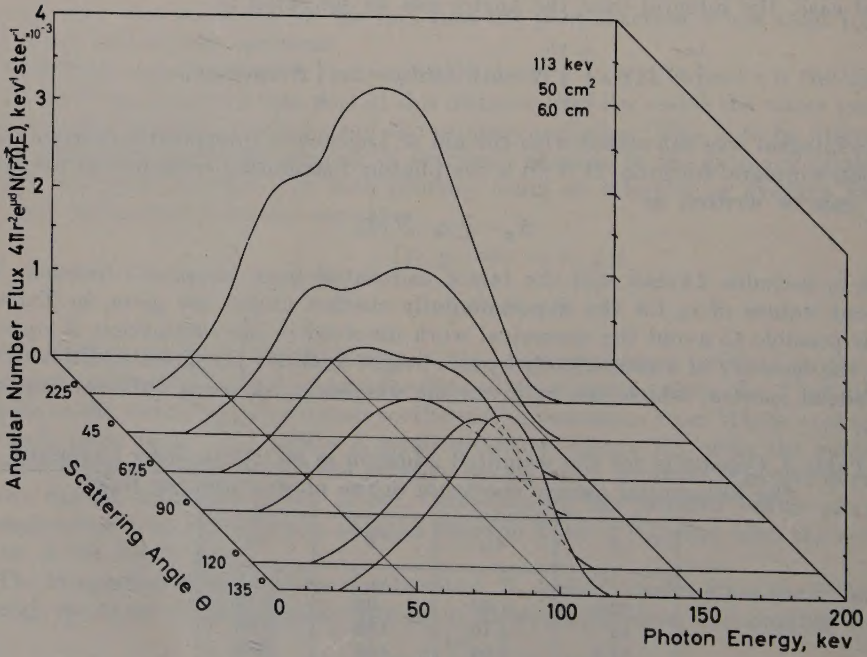
113 kev
50 cm^2
6.0 cm
Angular Number Flux $4\pi r^2 e^{\mu d} N(\vec{r}, \vec{\Omega}, E)$, kev^{-1}ster^{-1}
4
$\times 10^{-3}$
3
2
1
0
Scattering Angle Θ
22.5°
45°
67.5°
90°
120°
135°
0
50
100
150
200
Photon Energy, kev

6 b.

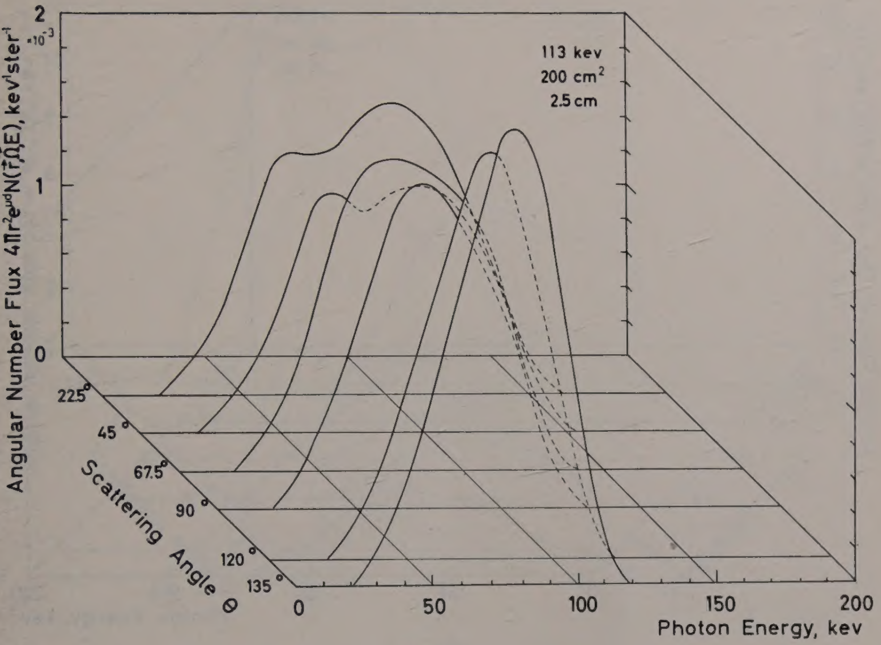
Angular Number Flux $4\pi r^2 e^{\mu d} N(\vec{r},\vec{\Omega},E)$, kev^{-1}ster^{-1}
$\times 10^{-3}$
2
1
0
113 kev
200 cm^2
2.5 cm
22.5°
45°
67.5°
90°
120°
135°
Scattering Angle Θ
0
50
100
150
200
Photon Energy, kev

7 a.

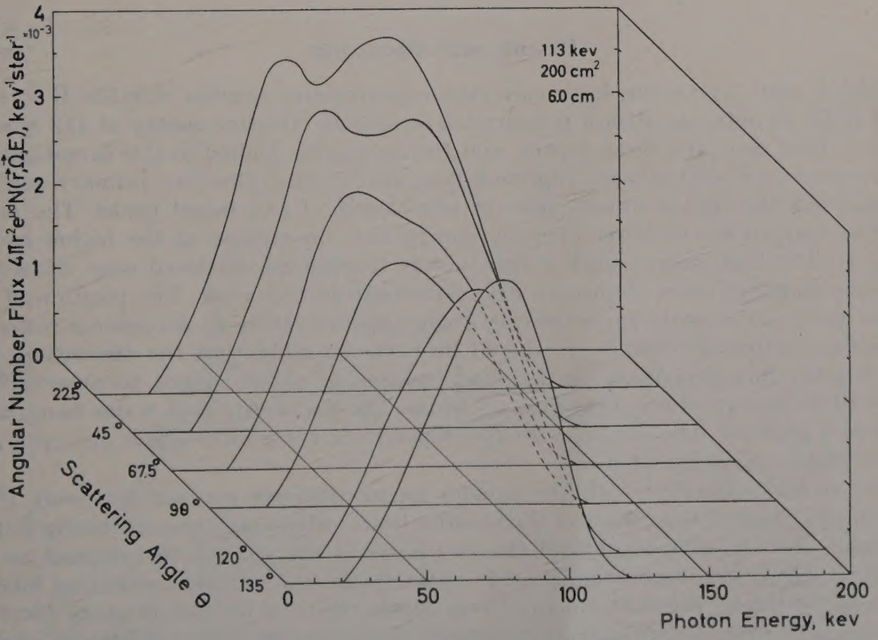
Angular Number Flux $4\pi r^2 e^{\mu d} N(\vec{r},\vec{\Omega},E)$, kev^{-1}ster^{-1}
$\times 10^{-3}$
4
3
2
1
0
113 kev
200 cm^2
6.0 cm
22.5°
45°
67.5°
90°
120°
135°
Scattering Angle Θ
0
50
100
150
200
Photon Energy, kev

7 b.

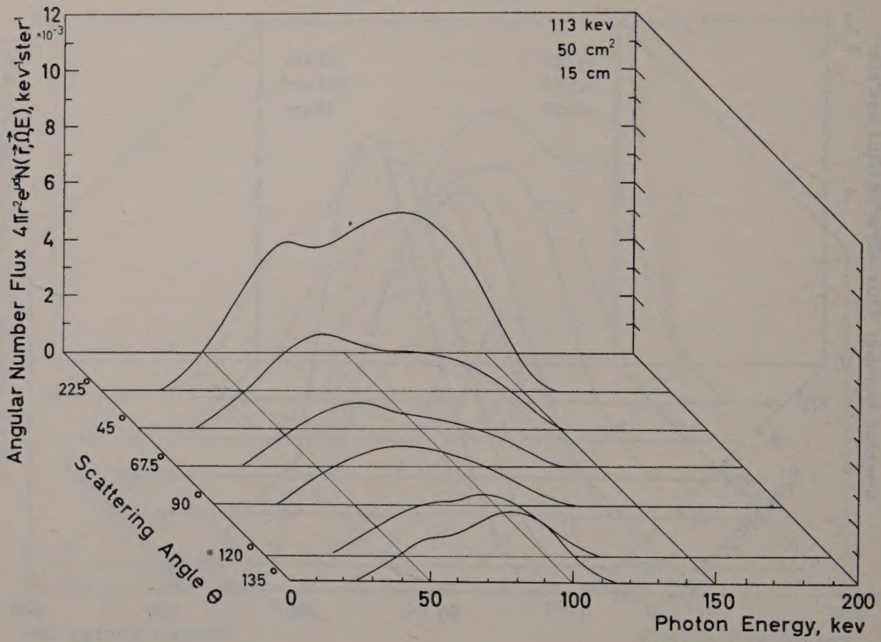

6 c.

Fig. 6 a–c. Angular number flux of the scattered radiation at three depths (2.5, 6.0, and 15 cm), for a primary beam with an effective energy of 113 kev and a field size of 50 cm².

Results and discussion

Figs. 6 and 7 give the fully corrected experimental angular number flux $4\pi r^2 e^{\mu d} N(\mathrm{r}, \mathbf{\Omega}, E)$ obtained with a primary beam with an effective energy of 113 kev for the two field sizes, the three depths, and the six angles studied in this investigation. These curves are qualitatively representative also for the other two primary energies studied. All the curves consist more or less clearly of two broad peaks. The peaks are less marked at the lower primary energy but conspicuous at the higher energy (Fig. 8). The high energy peak is due mostly to photons scattered once. However, photons scattered more than once also contribute to this peak. The position of the upper peak varies with the scattering angle approximately in accordance with the Compton scattering formula. It should be borne in mind that the discontinuity of the number flux depending on the single scattering cutoff cannot be observed because of the energy width of the primary beam. The low energy peak is due to multiply scattered photons. The cutoff at 20 kev depends on the photoelectric absorption in water of the degraded photons.

The spectra obtained with the smaller beam diameter contain relatively fewer low energy photons than those of the broader beam, where multiple scattering is more probable. The relative heights of the two parts of the spectra also depend on the depth at which the observation is made in the water, the multiple scattering increasing with the depth. For the 6 cm and 15 cm depths the total photon intensity decreases fairly rapidly with increasing scattering angle up to about 90°, after which it is approximately constant. This is, however, not the case at a depth of 2.5 cm with a 200 cm²

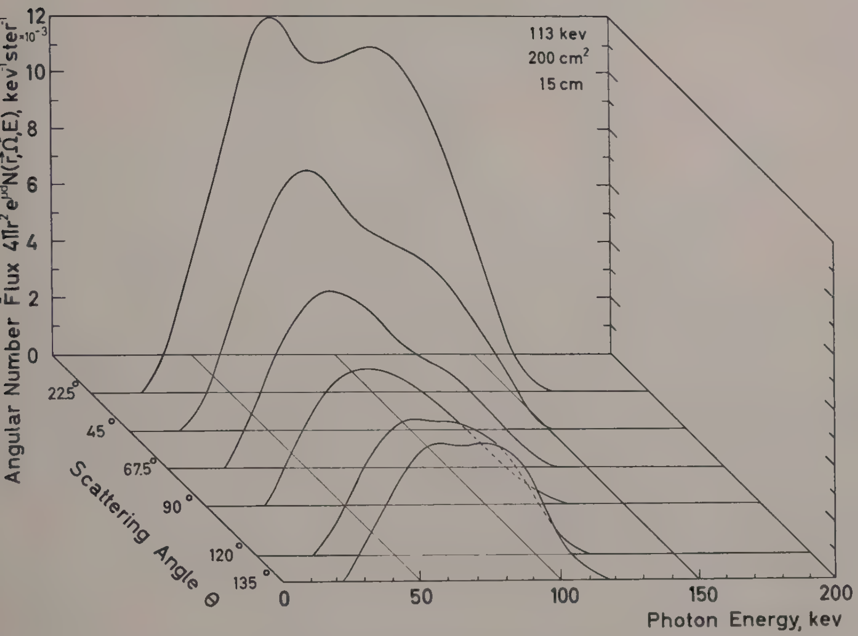

7 c.

Fig. 7 a–c. Angular number flux of the scattered radiation at three depths (2.5, 6.0, and 15 cm), for a primary beam with an effective energy of 113 kev and a field size of 200 cm².

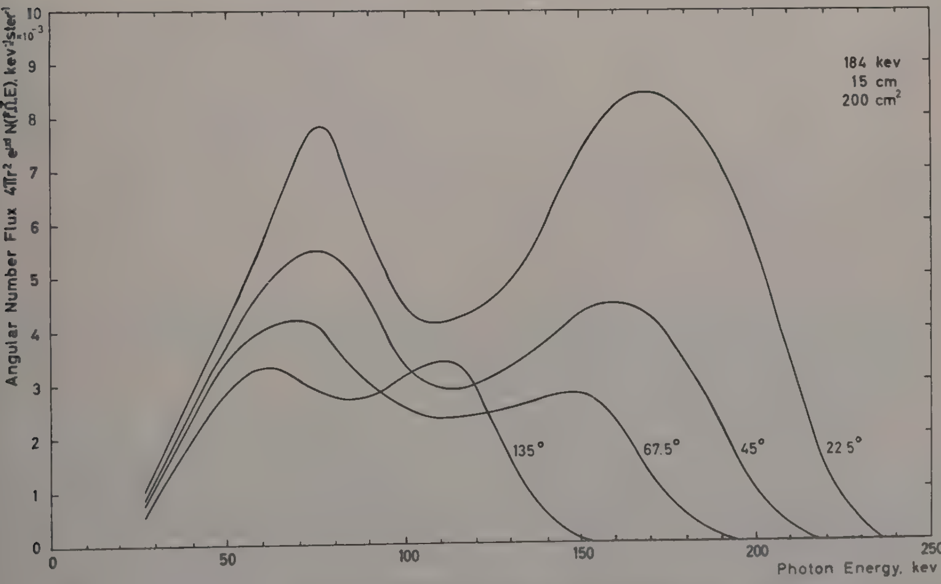

Fig. 8. The angular number flux of the scattered radiation at a depth of 15 cm and for a primary beam with an effective energy of 184 kev. The low energy peak due to multiply scattered radiation appears clearly and for scattering angles above 90° it is relatively fixed with a peak energy of about 60 kev.

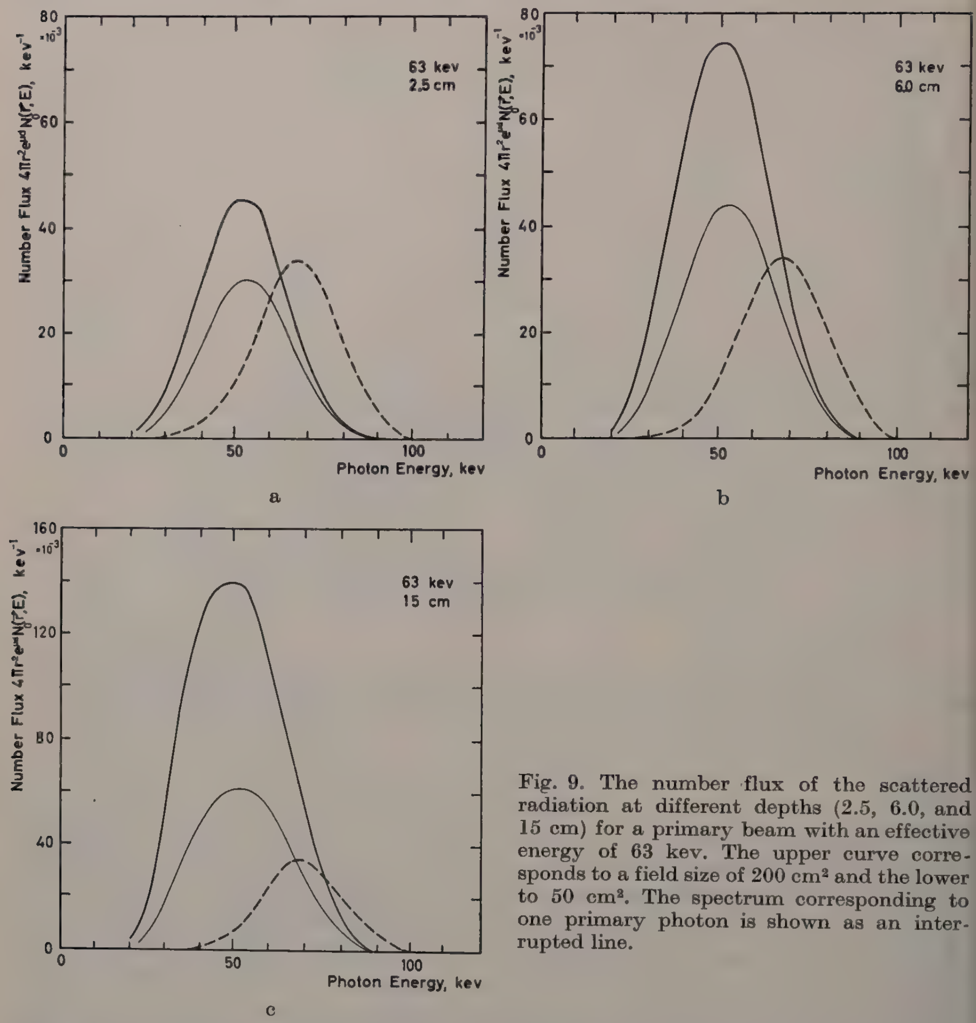

Fig. 9. The number flux of the scattered radiation at different depths (2.5, 6.0, and 15 cm) for a primary beam with an effective energy of 63 kev. The upper curve corresponds to a field size of 200 cm² and the lower to 50 cm². The spectrum corresponding to one primary photon is shown as an interrupted line.

field. The relatively low intensities at 22.5° and 45° are then due to the proximity of the surface of the phantom. The amount of water seen by the spectrometer is smaller at these angles than at 67.5°. The photon intensities at 22.5° and 45° do not change much with field sizes between 50 and 200 cm².

For the highest primary energy studied, the singly and multiply scattered photons are well separated in energy. The low energy peak can be studied in Fig. 8, where the angular number flux is plotted for the angles 22.5°, 45°, 67.5°, and 135°. The field size is 200 cm² and the depth 15 cm. In the diagram the 90° and 120° plots were excluded, because the low energy peak of these curves has almost the same energy and shape as that of the 135° curve. As seen in the diagram, the peak energy shows an obvious tendency to decrease with increasing angle of observation. This means that the average number of collisions of the photons is not sufficient for them to have lost the memory of their original direction. The number of collisions is highest for

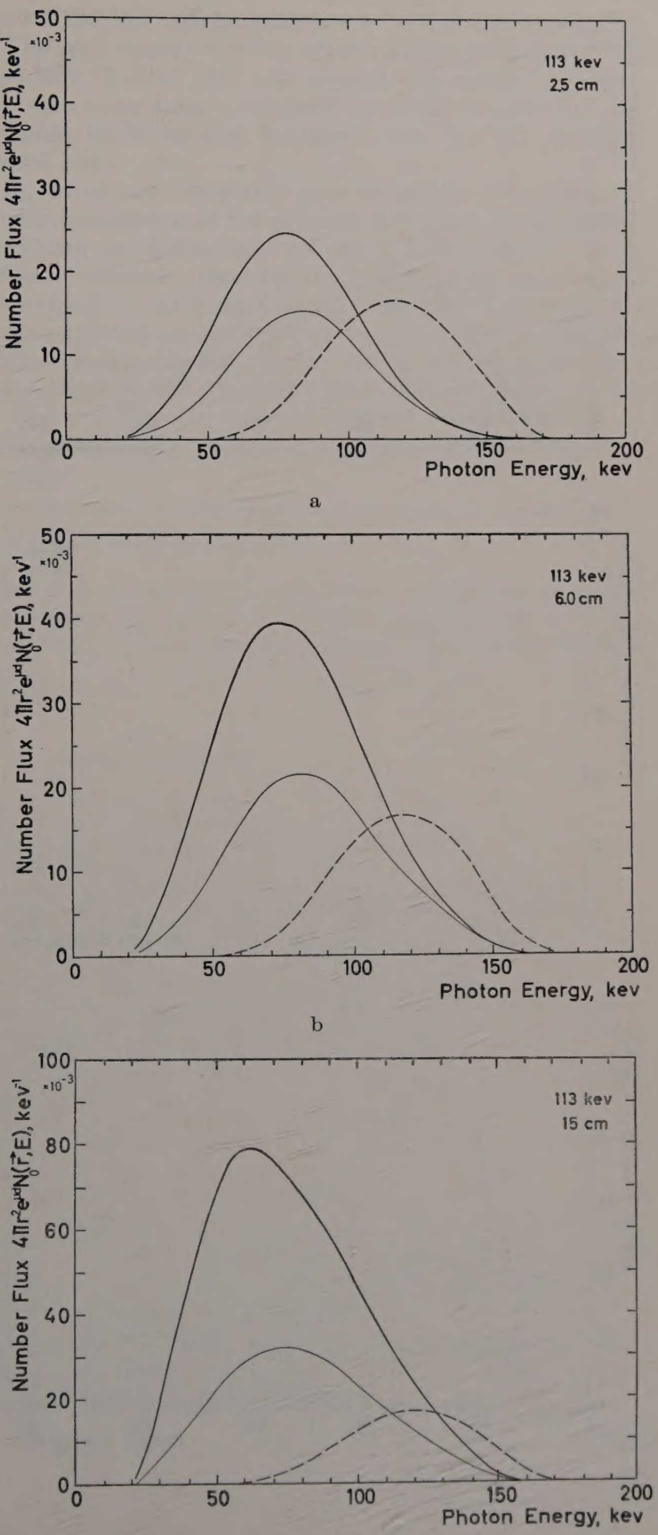

a

b

c

Fig. 10. The number flux of the scattered radiation at different depths (2.5, 6.0, and 15 cm) for a primary beam with an effective energy of 113 kev. The upper curve corresponds to a field size of 200 cm² and the lower to 50 cm². The spectrum corresponding to one primary photon is shown as an interrupted line.

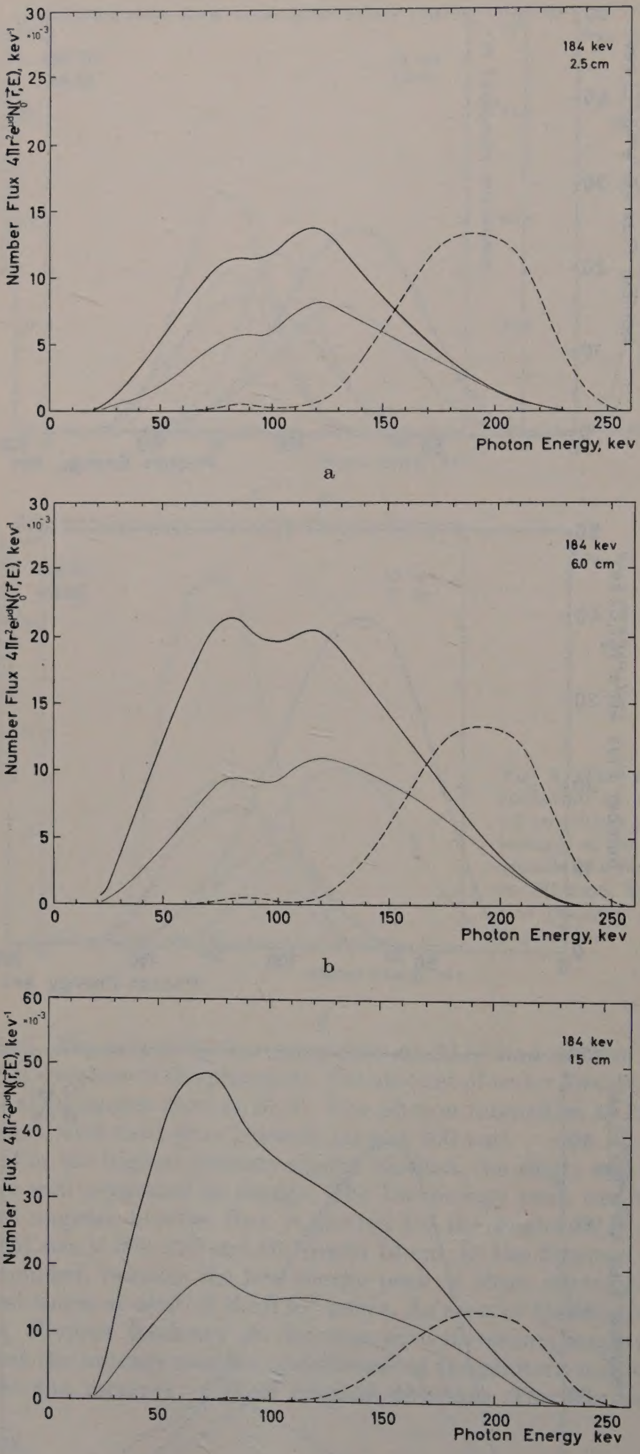

a

b

c

Fig. 11. The number flux of the scattered radiation at different depths (2.5, 6.0, and 15 cm) for a primary beam with an effective energy of 184 kev. The upper curve corresponds to a field size of 200 cm² and the lower to 50 cm². The spectrum corresponding to one primary photon is shown as an interrupted line.

the backscattered radiation, and the low energy peak lies at a constant energy for scattering angles above 90°. The peak energy is about 60 kev and in good agreement with that given by Hayward and Hubbel [23] who studied this energy region in the backscattered radiation from a wood target irradiated by cobalt-60 gammas. The theoretical spectrum as presented by Weiss and Bernstein [20], however, shows a peak energy somewhat below 50 kev.

The number fluxes $N_0(\mathbf{r}, E)$, which are integrated over all angles, are shown in Figs. 9, 10, and 11 together with the spectra of the primary radiations at the points of observation. The number fluxes are normalized for one primary photon. It is obvious that the softening effect of scattering upon the total photon spectra increases with the amount of water penetrated by the beam and with the size of the radiation field. The average energy of the scattered radiation relative to the primary spectrum is also seen to decrease with increasing primary photon energy. The diagrams also give a rough estimate of the increase in the photon buildup with the depth in the scattering medium.

Other radiation physical discussions of the present investigation will be treated in greater detail in a following paper.

ACKNOWLEDGEMENT

The authors wish to express their sincere gratitude to Dr. K. Lidén for suggesting the present investigation and also for constant support and many fruitful discussions throughout the entire investigation. This investigation has been supported by grants from the Swedish Cancer Society.

Radiation Physics Department, University of Lund, Lund, Sweden, June 1958.

REFERENCES

1. R. Payne-Scott, Brit. J. Radiol. *10*, 850 (1937).
2. L. V. Spencer and U. Fano, J. Res. Nat. Bur Standards *46*, 446 (1951).
3. L. V. Spencer and U. Fano, J. Res. Nat. Bur. Standards *51*, 95 (1953).
4. U. Fano, Nucleonics *11*, No. 8, 9 (1953) and *11*, No. 9, 55 (1953).
5. H. Goldstein and J. E. Wilkins, Jr., United States AEC, Report NYO-3075 (1954).
6. W. R. Bruce and H. E. Johns, Radiology *68*, 100 (1957).
7. J. O. Hirschfelder, J. L. Magee, and M. H. Hull, Phys. Rev. *73*, 852 (1948).
8. J. O. Hirschfelder and E. N. Adams, Phys. Rev. *73*, 863 (1948).
9. L. Cave, J. Corner, and R. H. A. Liston, Proc. Roy. Soc. *204*, 223 (1951).
10. J. Corner and R. H. A. Liston, Proc. Roy. Soc. *204*, 323 (1951).
11. G. H. Peebles, J. Appl. Phys. *24*, 1272 (1953); ibid. *24*, 1437 (1953).
12. E. H. Quimby and R. F. McNattin, Amer. J. Roentgenol. *28*, 236 (1932).
13. J. R. Clarkson and W. V. Mayneord, Brit. J. Radiol. *12*, 168 (1939).
14. C. W. Wilson, Brit. J. Radiol. *12*, 231 (1939).
15. J. R. Greening and C. W. Wilson, Brit. J. Radiol. *24*, 605 (1951).
16. J. R. Greening, Brit. J. Radiol. *24*, 204 (1951).
17. G. R. White, Phys. Rev. *80*, 154 (1950).
18. M. A. Van Dilla and G. J. Hine, Nucleonics *10*, No. 7, 54 (1952).
19. E. Hayward, Phys. Rev. *86*, 493 (1952).
20. M. M. Weiss and W. Bernstein, Phys. Rev. *92*, 1264 (1953).
21. R. B. Theus, L. A. Beach, and W. R. Faust, J. Appl. Phys. *26*, 294 (1955).
22. R. W. Peelle, F. C. Maienschein, and T. A. Love, ORNL-report No 2196 (1957).
23. E. Hayward and J. H. Hubbel, J. Appl. Phys. *25*, 506 (1954).
24. G. Hettinger and N. Starfelt, Acta Radiol. *50*, 381 (1958).
25. D. V. Cormack, T. J. Griffith, and H. E. Johns, Brit. J. Radiol. *30*, 129 (1957).
26. G. Hettinger and N. Starfelt, Nucl. Instr. *3*, 25 (1958).
27. G. White Grodstein, Nat. Bur. Standards Circular 583 (1957).

Tryckt den 12 januari 1959

Uppsala 1959. Almqvist & Wiksells Boktryckeri AB